J Mater Sci: Mater Med (2007) 18:25–37
DOI 10.1007/s10856-006-0659-8

Membrane thickness design of implantable bio-MEMS sensors for the *in-situ* monitoring of blood flow

C. A. Steeves · Y. L. Young · Z. Liu · A. Bapat · K. Bhalerao · A. B. O. Soboyejo · W. O. Soboyejo

Received: 20 October 2005 / Accepted: 28 February 2006

Abstract This paper presents some ideas for the membrane thickness design of of implantable bio-micro-electro-mechanical systems (bio-MEMS) for the *in situ* monitoring of blood flow. The objective is to develop a smart wireless sensing unit for non-invasive early stenosis detection in heart bypass grafts. The design includes considerations of nonlinear material models, multiscale blood flows, and appropriate analyical models for data interpretation, as well as preliminary studies of the pressure and flow sensing concepts. The paper also examines the use of surface coatings for the design on biocompatibility and non-adhesion of blood platelets and constituents. The implications of the results are discussed for *in vivo* deployment of such sensor systems.

C. A. Steeves (✉)
Department of Mechanical and Aerospace Engineering, Princeton University, Princeton, NJ 08544

Y. L. Young · Z. Liu
Department of Civil and Environmental Engineering, Princeton University, Princeton, NJ 08544

A. Bapat
Department of Chemical Engineering, McGill University, Montreal, Quebec, Canada

K. Bhalerao · A. B. O. Soboyejo
Department of Food, Agricultural and Biological Engineering, Ohio State University, Columbus, OH 43210

W. O. Soboyejo
Department of Mechanical and Aerospace Engineering, Princeton University, Princeton, NJ 08544

Introduction

Stenosis is the narrowing, stiffening, thickening, fusion, or blockage of a blood vessel. It is usually caused by fatty plaque buildup, and it can be an extremely serious problem particularly when the stenosis occurs in the blood vessels around the heart. A common procedure to treat stenotic heart arteries is coronary bypass surgery, which involves bypassing the blocked arteries by attaching another blood vessel proximal and distal to the blockage. In most cases, grafts (arteries or veins from another part of the body) are used to reroute the blood. Unfortunately, narrowing of the blood vessel used as a bypass graft is a common problem. Such stenosis can happen immediately after the surgery due to thrombosis (blood clot) triggered by tissue trauma, or within three to six months following the surgery due to tissue growth at the site of the treatment [1]. Stenosis can also occur due to recurrent atherosclerosis, the same reason that led to the original artery blockage. According to the report presented in [2], 20–30% of the bypass patients require another bypass within 10 years. Thus, surveillance methods are needed to detect stenosis and to prevent impending graft failure. Currently, available surveillance methods include catheter angiography (X-ray examination of the blood vessel by passing a catheter through an artery leading to the area of interest), and other less invasive methods such as computer tomography (CT) angiography, magnetic resonance (MR) angiography, and duplex ultrasound (combined Doppler and conventional ultrasound measure of the blood flow). However, these methods are either invasive, expensive, or operator dependent. In addition, they are not appropriate for extended monitoring of the grafts. The ultimate aim of the present study is to develop wireless bio-MEMS sensors for continual monitoring

of blood flow *in situ* which can be easily implanted during bypass surgery. The four specific goals of this work are:

- Develop a fluid model to estimate the degree of stenosis based on sensor readings.
- Develop a material model to investigate the effect of fatty plaque buildup and vessel wall characteristics on pressure measurements.
- Develop guidelines for the introduction of biocompatible surface coatings that will also resist adhesion of blood constituents.
- Investigate the feasibility of *in vivo* deployment of the proposed sensing unit.
- Develop guidelines for the design of an implantable bio-MEMS pressure sensor that is able to simultaneously satisfy sensitivity, biocompatibility, durability, and reliability requirements.

Fluid model

In the past five decades, the concept of "critical stenosis" has been widely adopted [3]. This implies that the blood flow rate may not significantly vary in a stenotic vessel until it reaches a critical state, i.e., 69–95% [4]. However, medical treatment will be too late when the "critical stenosis" is reached. On the other hand, other flow characteristics, including flow separation, pressure drop, and wall shear stresses, are much more sensitive to development of even mild stenosis. Thus, much of the past theoretical research focused on determining these detailed flow characteristics.

In May et al. [4], a simplified equation was developed to estimate the pressure drop across a stenosis by idealizing the geometry as a combination of sudden contraction, Poiseuille flow through a narrowed lumen, and a sudden expansion. The flow was assumed to be steady and non-pulsatile. Later, Young et al. [5] modified the pressure drop equation by considering the effects of stenosis size and shape, turbulence, and fluid acceleration via empirically derived coefficients. Based on the experimental data, Young et al. [5] found that the mean pressure drop generally increased while the flow rate decreased as the stenosis increased in severity.

Since the early 1970's, computational fluid dynamics (CFD) models were also developed to investigate flow characteristics in idealized stenotic arteries (for early examples, see [5–12]). Recent examples include the works of Tu et al. [11], Dvinsky and Ojha [13], Tu and Deville [14], Ghalichi et al. [15], Bluestein et al. [16], Tura and Cavalcanti [17], Mallinger and Drikakis [18], Varghese and Frankel [19], Guotao et al. [20], which considered the effects of pulsatile inflow, non-Newtonian blood flow, and turbulence. Most recently, the effects of fluid-structure interactions have also been considered by Tang et al. [21] and Moayeri and Zendehbudi [22]. However, most of these models focused on determining pressure and flow field for a given stenosis geometry. In this work, the objective is to estimate the percentage stenosis based on limited pressure and flow measurements from implanted bio-MEMS sensors. An axisymmetric CFD model is developed to serve as a "virtual testing device" to simulate the pressure drop across varying degree of stenosis. A simplified equation based on coefficients derived from the numerical simulations is then developed to relate the sensor readings to the degree of stenosis. Details of the flow solver and the formulation of the simplified equation are given below.

Axisymmetric CFD model

The blood flow through a stenotic vessel is assumed to be laminar, incompressible, axisymmetric, and Newtonian, which has been shown to yield satisfactory estimates of the global flow characteristics; for example, see [6, 7, 9, 23–25]. The non-dimensionalized governing equation can be written as:

$$\frac{\partial \omega}{\partial t} + \frac{\partial}{\partial x}(u\omega) + \frac{\partial}{\partial r}(v\omega) = \frac{1}{Re}\left(\frac{\partial^2 \omega}{\partial x^2} + \frac{\partial^2 \omega}{\partial r^2} + \frac{1}{r}\frac{\partial \omega}{\partial r} - \frac{\omega}{r^2}\right) \tag{1}$$

$$-\omega = \frac{1}{r}\left(\frac{\partial^2 \psi}{\partial x^2} + \frac{\partial^2 \psi}{\partial r^2} - \frac{1}{r}\frac{\partial \psi}{\partial x}\right) \tag{2}$$

where

$$\omega = \frac{\partial v}{\partial x} - \frac{\partial u}{\partial r}; \quad u = \frac{1}{r}\frac{\partial \psi}{\partial r}; \quad v = -\frac{1}{r}\frac{\partial \psi}{\partial x} \tag{3}$$

and the non-dimensional variables are defined as:

$$r = \frac{r^*}{R}; \quad x = \frac{r^*}{R}; \quad u = \frac{u^*}{U_0}; \quad v = \frac{v^*}{U_0}; \quad \omega = \frac{\omega^*}{U_0/R};$$
$$\psi = \frac{\psi^*}{U_0 R^2}; \quad p = \frac{p^*}{\rho U_0^2}; \quad Re = \frac{\rho U_0 R}{\mu}; \quad t = \frac{t^*}{R/U_0} \tag{4}$$

x and r are the axial and radial coordinates, respectively; u and v are the axial and radial velocity components, respectively; ρ is the blood density; U_0 is the peak inflow velocity; R is the inner radius of the blood vessel; and μ is the dynamic viscosity.

Defining p as the static pressure, the total pressure $P \equiv p + \frac{1}{2}(u^2 + v^2)$ can be expressed as a function of the velocity

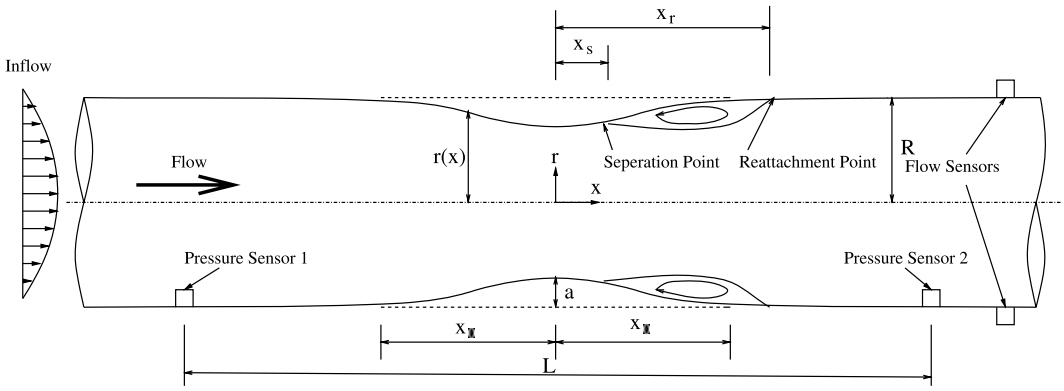

Fig. 1 Geometries of stenosis

and vorticity:

$$\frac{\partial P}{\partial x} = v\omega - \frac{1}{Re}\left(\frac{\omega}{r} + \frac{\partial \omega}{\partial r}\right). \tag{5}$$

Applying the no slip condition, the pressure on the wall can be obtained by integrating the following differential equation:

$$\frac{\partial P}{\partial x} = -\frac{1}{Re}\left(\frac{\omega}{r} + \frac{\partial \omega}{\partial r}\right). \tag{6}$$

Following the work of Young and Tsai [7] , the geometry of stenosis is assumed to be axisymmetric, and is described by the following equation:

$$\begin{aligned} r(x) &= 1 - \frac{a}{2}\left[1 + cos\left(\frac{\pi x}{x_0}\right)\right]; \quad (-x_0 \le x \le x_0) \\ r(x) &= 1; \quad (|x| \ge x_0). \end{aligned} \tag{7}$$

A graphical depiction of the model geometry is shown in Fig. 1. A parabolic velocity profile is assumed at the inflow boundary. The axisymmetric flow condition is applied at the centerline, and the no-slip condition is applied at the vessel wall. The second derivatives of the stream function and vorticity are assumed to be zero at the outflow boundary.

To validate the model, the numerical predictions are compared with numerical predictions presented in [9] and experimental measurements presented by Young and Tsai [7]. The predicted stream functions and vorticity contours for model M1 ($\alpha = 24$, $\beta = 56\%$, $Re = 100$) are shown in Figs. 2 and 3, respectively, both of which compared well with predictions obtained by Deshpande et al. [9]. As shown in Fig. 4, the predicted pressure drop as a function of the Reynolds number also compared well with experimental measurements presented by Young and Tsai [7].

The objective of the axisymmetric CFD solver is to simulate blood flow across varying degrees of stenosis to develop a simplified relationship between the percentage stenosis and pressure drop across two fixed bio-MEMS sensors. An example of the predicted pressure profile for varying degree of stenosis is shown in Fig. 5. The throat of the stenosis is located at $x = 0$. The length (x_0) to thickness (a) ratio of the stenosis, $\alpha \equiv x_0/a$, is assumed to be 10, and the percentage stenosis, β, is defined as:

$$\beta \equiv \frac{A_0 - A_1}{A_0} \times 100\% \tag{8}$$

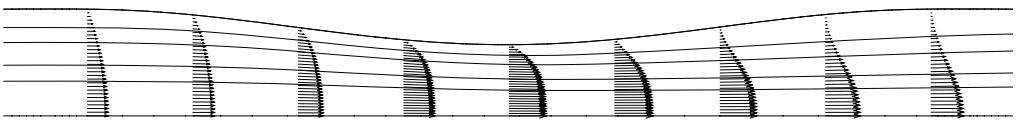

Fig. 2 Stream function contours for model M1, Re = 100

Fig. 3 Vorticity contours for model M1, Re = 100

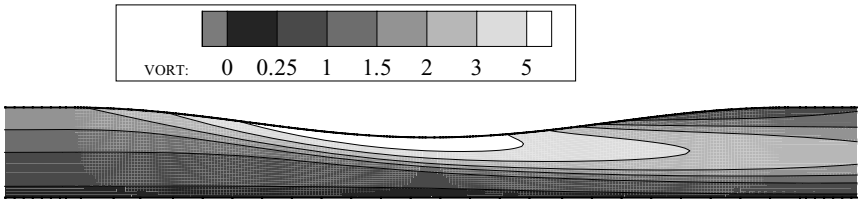

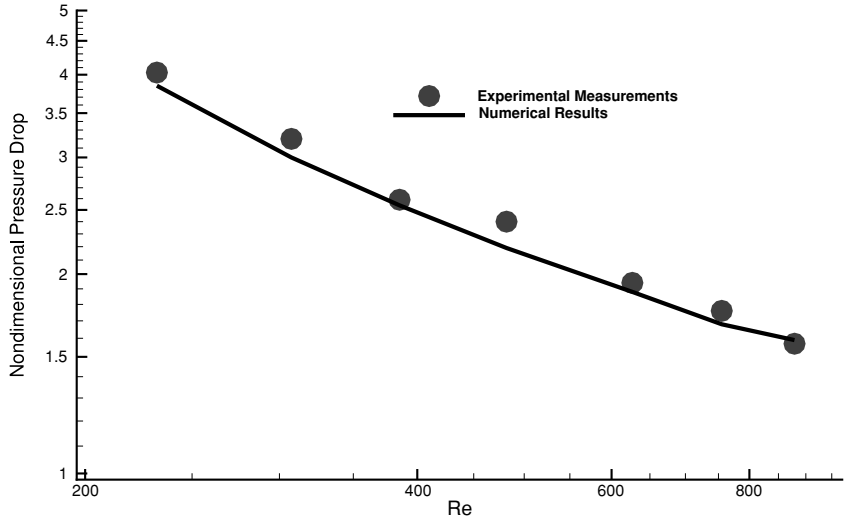

Fig. 4 Comparison between numerical results and experimental measurements in [7] (Model M1)

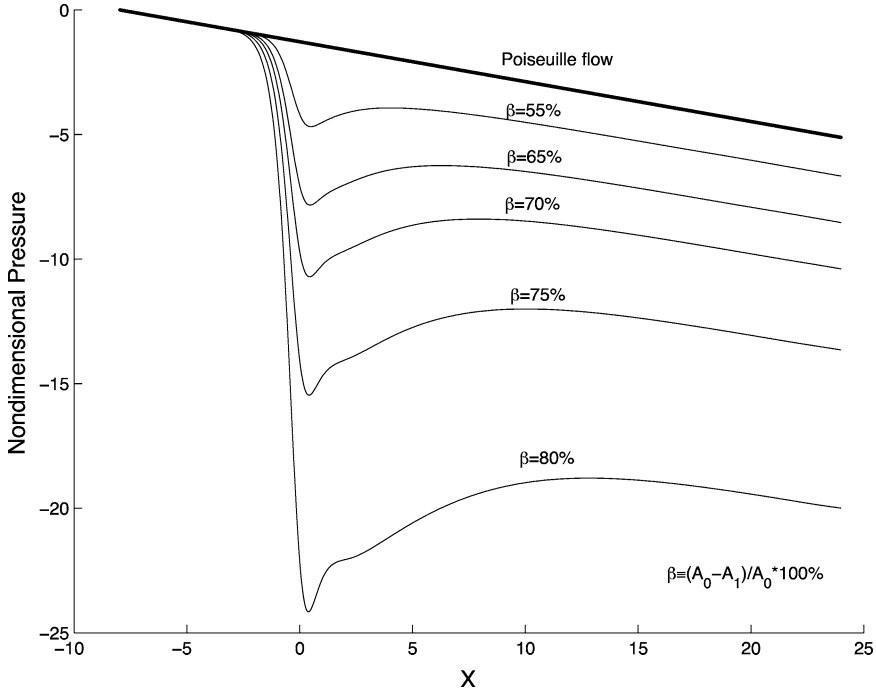

Fig. 5 Pressure profile at the wall for varying degree of stenosis ($\alpha \equiv \frac{x_0}{a} = 10$)

where $A_0 = \pi R^2$ is the unobstructed area and $A_1 = \pi(R - a)^2$ is the throat area as shown in Fig. 1. As expected, the pressure drop increases with the percentage stenosis, and the slope downstream of the flow reattachment point recovers to the value that corresponds to Poiseuille flow.

Simplified pressure equation

The objective of the simplified pressure equation is to relate the difference in pressure readings between two fixed sensors and the percentage stenosis. The wireless bio-MEMS sensors can be implanted on the interior surface at the two ends of the vessel with a wireless magneto-hydrodynamic flow sensor to continuously monitor blood flow *in situ.* A schematic diagram showing the placement of the sensors is shown in Fig. 1. The objective is to provide early detection and warning of stenosis, which can often occur due to thrombosis, excessive tissue growth, or recurrent atherosclerosis.

Denoting the pressure at the upstream and downstream sensors as p_1 and p_2, respectively, the pressure drop across the two sensors, $\Delta p \equiv p_2 - p_1$, can be decomposed into two parts:

$$\Delta p = \Delta p_v + \Delta p_t, \tag{9}$$

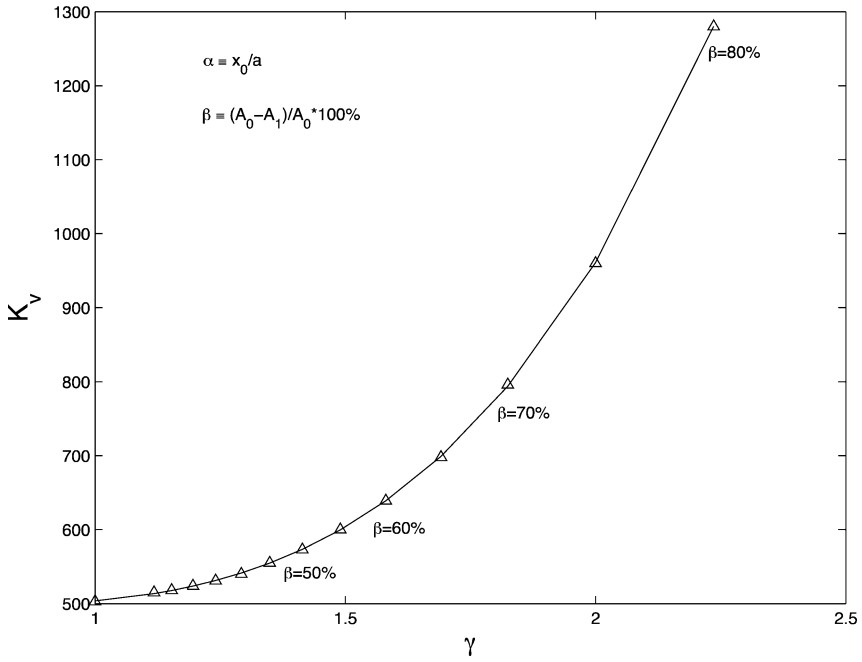

Fig. 6 Dependence of viscous coefficient on length ratio

where Δp_s is the pressure loss due to viscosity and Δp_t is the pressure loss due to turbulence.

Following the work of Young [3], Δp_v can be expressed in terms of the viscous coefficient, K_v, and Δp_t can be expressed in terms of the turbulence coefficient, K_t:

$$\Delta p_v = \frac{K_v}{Re}, \tag{10}$$

$$\Delta p_t = \frac{K_t}{2}\left(\frac{A_0}{A_1} - 1\right)^2. \tag{11}$$

It should be noted that the unsteady effect due to the fluid acceleration has been neglected in (9). Based on studies presented by Young [3], the unsteady effect is proportional to the rate of change of the mean velocity. Thus, Eq. (9) is valid if the time-averaged (over each flow cycle) pressure and flow readings are used.

Since the geometry of the stenosis is generally smooth (i.e. no abrupt corners or sudden geometric discontinuities), K_t can be assumed to be 0.9 for most cases [7]. Combining Eqs. (9), (10), and (11), K_v can be written as:

$$K_v = Re\left[\Delta p - 0.45\left(\frac{A_0}{A_1} - 1\right)^2\right]. \tag{12}$$

For a parabolic inflow velocity profile, K_v can be shown to be a fourth order function of the area ratio, $\gamma \equiv \sqrt{\frac{A_0}{A_1}}$:

$$K_v = \sum_{i=0}^{4} k_i \gamma^i, \tag{13}$$

where k_i is the ith coefficient of the 4th order polynomial for K_v.

By performing a series of numerical simulations using the developed axisymmetric CFD solver for varying degree of stenosis, the coefficients, k_i, can be extracted using least-square fit. Assuming the length to thickness ratio ($\alpha \equiv x_0/a$) of the stenosis to be 10, the simulated values from the CFD solver and the best fit curve of K_v for varying γ is shown in Fig. 6. The resulting fourth-order polynomial for K_v is:

$$K_v = 504.6 + 24.13\gamma - 67.5\gamma^2 + 0.16\gamma^3 + 42.28\gamma^4. \tag{14}$$

Combining Eqs. (9), (10), (11), and (13), the following relationship between Δp and γ can be obtained:

$$\Delta p = \sum_{i=0}^{4} p_i \gamma^i. \tag{15}$$

Thus, for a given p_1 (pressure at the upstream sensor), p_2 (pressure at the downstream sensor), and Q (flow rate), the degree of stenosis, $\beta \equiv \frac{A_0 - A_1}{A_0} \times 100\%$, can be determined by evaluating the root of Eq. (15). In other words, this equation can be used to interpret the percentage stenosis based on *in situ* sensor readings. To verify Eq. (15), *in vitro* testing can be conducted. For *in vivo* deployment, Eq. (15) should be modified to include the dependence of the flow rate on the degree of stenosis and the fluid-structure interaction between the flow and elastic motion of the arteries. Both effects are discuss in detail in the next section. Methodologies to include these two effects are also discussed.

Material model

The bio-MEMS pressure sensor should be implanted on the interior surface of the vessels to provide maximum sensitivity to changes in pressure due to early stenosis formation. However, it is possible that the sensor may itself become covered with an atheromic plaque. The utility of an implanted pressure sensor will depend upon the ability to diagnose accurately the formation of atherosclerotic plaques on the sensors themselves. Hence, a simplified material model is developed to investigate the sensitivity of the pressure measurements when obstructed by plaque formation.

Formulation

The artherosclerotic artery is idealized as a set of nested cylinders (shown in Fig. 7) with a pressure sensor placed at the interface between the aterial wall and the atheromous plaque. In past numerical studies, most models assumed the arteries to behave as membranes (see Fung [26]), thus ignoring the stress distribution across the thickness of the arterial wall. However, this radial stress distribution is the most important parameter that influences the pressure felt by a sensor at the interface between the artery and the atherosclerotic plaque. In the current work, the cross-section of the artery is assumed to be axisymmetric, and the axial stress, σ_{xx},is assumed to be zero, thus reducing the problem to one-dimension. In addition, two important simplifications are made: first, the viscous properties of the plaque and artery are ignored; second, the stress through the plaque and artery is assumed to be zero when the internal pressure is zero.

The artery is assumed to be subject to an internal pressure p, and zero external pressure. The radial stress σ_{rr} and the circumferential stress $\sigma_{\theta\theta}$ vary with the radial position r. The axisymmetric equilibrium equation in polar coordinates is:

$$\sigma_{\theta\theta} = \sigma_{rr} + r\frac{\partial \sigma_{rr}}{\partial r}. \tag{16}$$

where the radial and circumferential strains, ϵ_{rr} and $\epsilon_{\theta\theta}$, respectively, are defined as:

$$\epsilon_{rr} = \frac{\partial u_r}{\partial r} \quad \text{and} \quad \epsilon_{\theta\theta} = \frac{u_r}{r} \tag{17}$$

and u_r is the radial displacement.

The relationship between stress and strain is assumed to be nonlinear, and is of the form $\sigma = \sigma(\epsilon)$. The discretized first-order approximation of the radial and circumferential stresses can be expressed as follows:

$$\sigma_{rr}^{t+1} = \sigma_{rr}^{t} + E_r^t \Delta\epsilon_{rr}^t \tag{18}$$

$$\sigma_{\theta\theta}^{t+1} = \sigma_{\theta\theta}^{t} + E_\theta^t \Delta\epsilon_{\theta\theta}^t \tag{19}$$

where the superscripted t denotes the step number. The strain-dependent tangential Young's moduli in the radial direction, E_r, and the circumferential direction, E_θ, are extracted from the stress-strain relations for the plaque and the artery wall. The governing equations are then solved incrementally using the linearized constitutive law. This model has been validated with analytical solutions for an isotropic elastic cylinder and a cylinder composed of two nested isotropic materials. At the material discontinuity between the plaque and the artery wall, there is a small numerical oscillation of magnitude approximately 1% of the total pressure variation through the plaque and arterial wall. This oscillation was determined to be negligible and hence has not been suppressed by the addition of artificial numerical viscosity.

Material constitutive relations

Both the atheroma and the arterial wall are idealized as non-linear anisotropic elastic media, with constant properties through their thicknesses. Only the radial and circumferential stresses are considered because plane stress is assumed. Biaxiality of the loading is ignored, principally due to the lack of biaxial material data for the radial—circumferential interaction; this is equivalent to setting the Poisson's ratio $\nu_{r\theta} = 0$.

The importance of the mechanical properties of arterial tissue has long been recognized and has been measured since the latter part of the nineteenth century [27]. Bergel [28] systematically addressed mechanical testing of arteries, and pointed out that both the nonlinearity of the stress-strain relation, and the variation in mechanical properties between different arteries and subjects. Patel et al. [29] provided some of the only multiaxial through-thickness compressive data

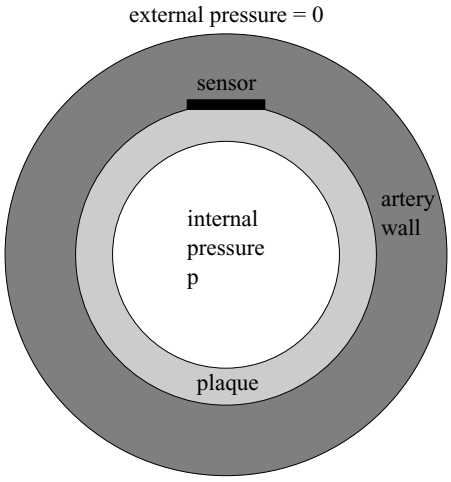

Fig. 7 Sketch of the idealised artery with sclerotic plaque

available, although their work was on canines. A number of authors have examined the progression of the stiffness of a plaque through time as high-cholesterol diets were fed to animals, but treated the stress-strain relation as linear; see Castle and Gow [30], Gow et al. [31], or Matsumoto et al. [32]. The nonlinear data supplied by Loree et al. [33] for the circumferential moduli of plaques and arteries is inconsistent with other reported data, being approximately on order of magnitude stiffer. Fung [26] provides extensive nonlinear data on the variation on arterial material properties in dogs, but not in humans. Hayashi and Imai [34] reports on a finite element model of the stresses in an artery affected by atheromatous plaque. They measure useful nonlinear material properties, but model the artery and plaque as isotropic. Salunke and Topoleski [35] review the existing literature and concluded that the material properties of atherosclerotic plaque are poorly characterized. In summary, there is a general lack of reliable and consistent data for the constitutive laws for both the arterial wall and the sclerotic plaque, the reasons being:

1. There is a wide range of material properties even for the same biological structure for the same subject. For example, Fig. 8.2:2 in Fung [26] shows the large variability of material properties in a single aorta with the location from which the sample was taken.
2. There are substantial histological differences between the same structure in different test subjects, and in the same subject at different times. Atherosclerotic plaques, for example, progress over time from relatively com pliant non-fibrous plaques to stiffer fibrous plaques, and finally to calcified plaques which are the stiffest of the three; see Lee et al. [36].
3. Different authors have used a variety of test methods and data reduction techniques to measure the same property, often arriving at very different results; see Hayashi [37].
4. The size of the available specimens has prevented the measurement of the most salient data, and an alternate measurement has been substituted. For example, Patel et al. [29] did not have the capacity to measure the radial strain in compression and had to infer it from other tests.
5. In some instances, the authors have treated the materials as linear elastic, and hence characterised by a single modulus of elasticity; see Castle and Gow [30] or Lee et al. [38]. This is clearly inadequate.
6. The measured properties have been for stress states far outside the normal physiological conditions; see Loree et al. [33] or Topoleski and Salunke [39].

These deficiencies exist for both the arterial wall and for the atherosclerotic plaque, but are particularly severe in the case of the plaque. In this work, the data for non-fibrous (or cellular) plaques is employed, as these are the earliest morphology of plaque and hence the first to have an impact upon sensor operation. The material data from Lee et al. [38] is used for the radial properties of the plaque, and from Hayashi and Imai [34] is used for the circumferential properties. Similarly, the data from Patel et al. [29] is used for the radial properties of the arterial wall, and from Hayashi and Imai [34] for the circumferential properties. The resulting four stress-strain curves are shown in Fig. 8. Both tensile and compressive stresses and strains are shown as positive to fit all the data into one quadrant. Note that the data from Lee et al. [38] for the radial properties of the plaque is limited to a single modulus of elasticity; following Fung [26] a non-linear region was assumed below 20 kPa in order to reduce the material discontinuites at low stresses and permit numerical convergence. Further, note that the radial arterial properties of Patel et al. [29] are taken from data for canines. Some human data is available in literature, but is limited to single value moduli of elasticity. A significant contribution to the literature can be made by performing accurate and

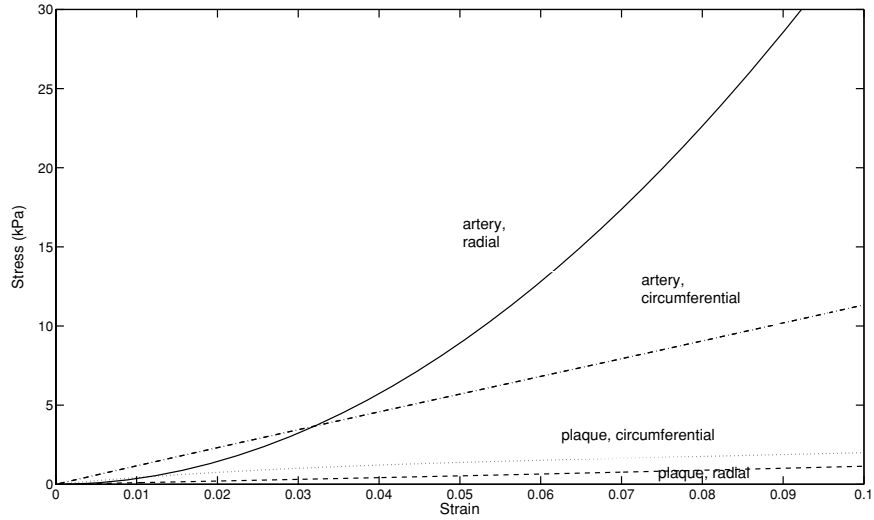

Fig. 8 Stress—strain relations for the arterial wall and atheromous plaque. Note that the radial properties are for compression but are shown as positive to retain all data in one quadrant

consistent measurements of the biaxial constitutive law for the arterial wall and the atherosclerotic plaque.

Results

To show the effect of a plaque progessively covering an *in vivo* pressure sensor, the variation in stress through the thickness of the plaque and artery, and at the surface of the artery for varying thicknesses of plaque growth, is shown in Fig. 9. The data in the figure correspond to a constant internal arterial pressure of 16 kPa for a 1 mm thick artery of 2 mm internal radius. The value of the pressure reading for a sensor located at the interface between the plaque and arterial wall, again for a constant internal pressure of 16 kPa, is given in the inset to Fig. 9. Note that the 1 mm plaque represents a 75% loss of arterial area. The reduction in pressure at the sensor is a slightly non-linear function of the thickness of the overlying plaque for this range of plaque thicknesses.

The deformation of the artery increases with the internal pressure. Figure 10 shows the external radius of an artery with initial unpressurized 2 mm inner radius and 3 mm external radius, subject to increasing internal pressure, for a selection

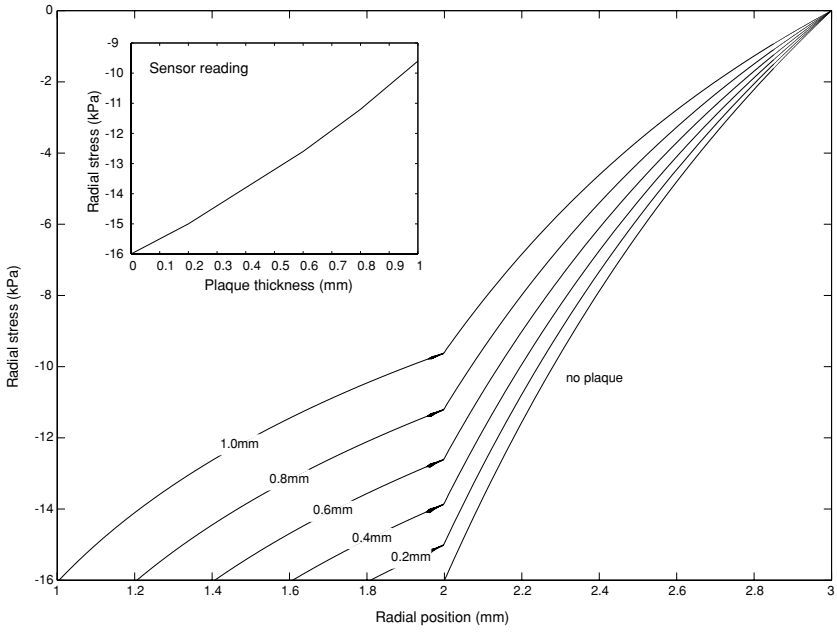

Fig. 9 Distribution of radial stress through the thickness of the plaque and arterial wall for various thicknesses of atheromous plaque on a 1 mm thick artery with 2 mm internal radius. The inset shows the radial stress at the interface between the plaque and the arterial wall

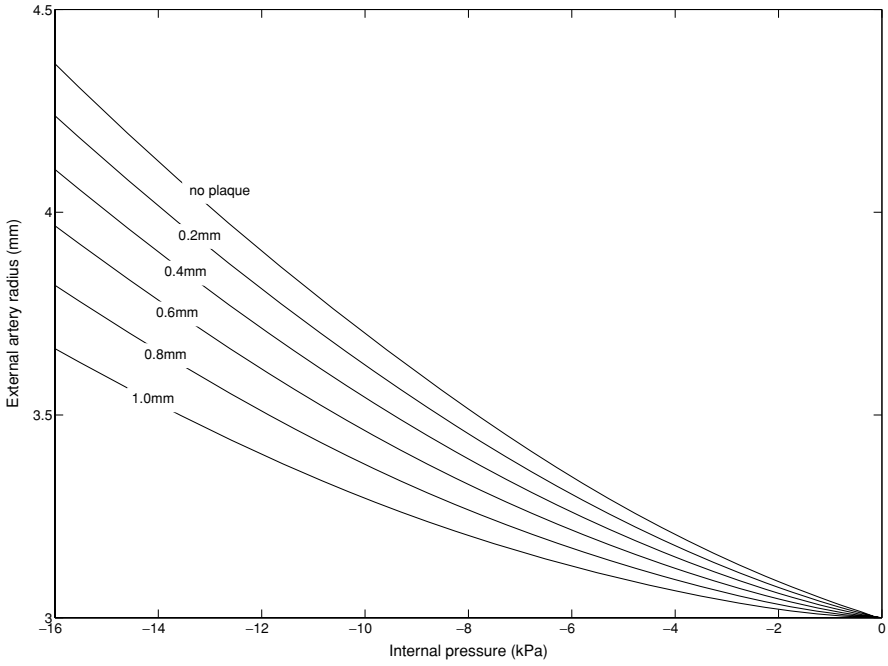

Fig. 10 External radius of an artery of 2 mm initial internal radius and 3 mm initial external radius, subjected to a range of internal pressures and obstructed by stenoses of various thicknesses

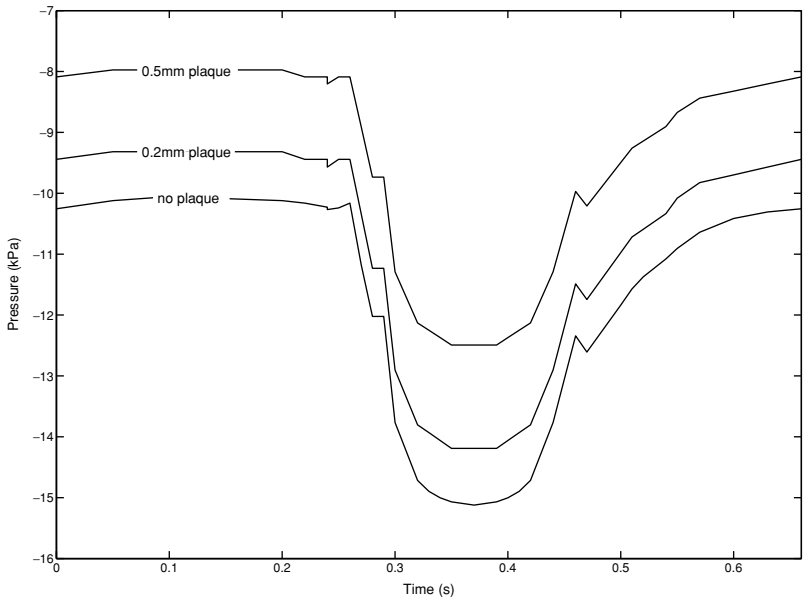

Fig. 11 Time—pressure relation for an arterial graft near the aorta for unobstructed arteries and for increasing obstruction by atheromous plaque

of plaque thicknesses. The hydraulic consequences of the expansion of the artery under pressure are an increase in flow for the same inlet pressure, and a reduction in the energy loss due to wall friction. Note that this model exaggerates the total change in the radius of the artery; the initial radius is taken for the zero pressure state, while for a natural artery the diastolic pressure would not drop below approximately 6 kPa. As the plaque thickness increases, the total deformation decreases, as expected.

Figure 11 shows the time—pressure curve for an unobstructed aorta over one heart beat; these data are taken from Fung [40]. A bypass graft typically leads to the heart from the aorta or a blood vessel near the aorta, and hence the aortic pressure can be taken as a good approximation to the actual pressure in the bypass graft. The time—pressure relations of pressure readings by sensors obstructed by atheromous plaque of several thicknesses are given in the same figure. Clearly the pressure sensor provides intelligible data despite obstruction by growing plaque.

Biocompatibility and bio-MEMS pressure sensing/reliability

The actual sensing of the local pressure in the blood vessel can be done using bio-MEMS (micro-electro-mechanical systems) pressure sensors [41, 42], similar to those shown in Fig. 12. A wide range of such sensors has been developed for the measurement of the blood pressure [41–43]. However, these are typically fabricated from silicon, which is not the most biocompatible material for long term use in the human body. There is, therefore, the need to develop coatings that can be used to improve the biocompatibility and long

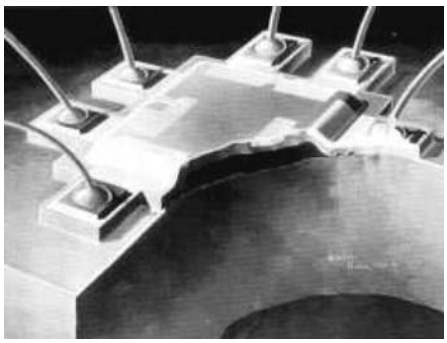

Fig. 12 A MEMS pressure sensor

term performance of implantable bio-MEMS pressure sensors. There is also a need to consider the sensing capability of possible sensor configurations that could be used to measure blood pressure *in-situ*. This section discusses the use of diaphragm sensors in the *in situ* measurement of blood pressure. It also examines the potential use of titanium and glycalyx layers in the coating of silicon for improved biocompatibility and the design of non-adhesion.

Pressure sensing

In this work, the use of implantable diaphragm sensors in the measurement of blood pressure is investigated. These sensors were first proposed about two decades ago [42], and have been used recently in the *in situ* monitoring of blood pressure in animals [43]. An example of a blood pressure sensor is presented in Fig. 12. This consists of a silicon bio-MEMS substrate with a thin layer of piezoelectric material. The membrane deflects due to the application of pressure, and the deflection gives rise to a wireless receiver at a

local or remote site [43]. In this way, the possible onset of stenosis and restenosis can be detected using an implantable pressure sensor.

The mechanics of sensing relies strongly on membrane mechanics. For a circular diaphragm mounted on an *O*-ring, the maximum deflection, δ, of the membrane is given by Timoshenko [44]:

$$\delta = \frac{Pa^4(5+\nu)}{64D(1+\nu)}, \tag{20}$$

where P is the pressure on the membrane, ν is the Poissons ratio, and a is the radius of the membrane. The variable D is given by:

$$D = \frac{Et^3}{12(1-\nu^2)}, \tag{21}$$

where t is the membrane thickness and E is the Young's modulus of the silicon layer. For silicon bio-MEMS, typical values of E are between 150 GPa and 220 GPa [45, 46]. The variability is due largely to variables in micro-texture [46] arising from differences in bio-MEMS fabrication schemes. In any case, an average Young's modulus of 175 GPa can be used for design estimates. For silicon bio-MEMS thin films, typical values of film thickness are in the range between 1 μm and 20 μm [41, 42]. Hence, Eqs. (20) and (21) can be combined to develop some criteria for bio-MEMS pressure sensing. Predictions of diaphragm deflection are presented in Fig. 13 for a range of clinically relevant pressures. These show that, for a 1 mm diameter pressure sensor, detectable deflections exist for normal biological pressures provided the membrane is less than approximately 20 μm thick. The transduced pressures can be converted to voltage output through the use of system functions that relate voltage output to pressure or membrane deflection.

It is important to note here that the optimal membrane thickness will depend on a complex range of parameters such as residual stresses and surface stresses arising from titanium coatings and protein absorption/interactions. These are difficult to quantify in the absence of experimental measurements and reliable theoretical models for the accurate prediction of such stresses. Hence, further experimental work is needed to establish the residual stresses and internal stresses that can affect the membrane deformation in actual bio-MEMS scenarios that are relevant to pressure detection. These are clearly beyond the scope of the current work.

bio-MEMS reliability

The maximum moment, $M_{\max}$, and the maximum bending stress, $\sigma_{\max}$, are also given respectively by:

$$M_{\max} = \frac{Pa^2(3t\nu)}{16} \tag{22}$$

$$\sigma_{\max} = \frac{6M_{\max}}{t^2}. \tag{23}$$

Since silicon has been shown to exhibit susceptibility to failure [47–52], the design objective should be to fabricate structures with stresses below the endurance limit, σ_e. Since there is no existing data for poly silicon bio-MEMS in biomedical environments, a further knock-down factor, α, must be applied to the design of reliable silicon pressure sensors. This gives the fatigue design condition as:

$$\sigma_{\max} < \frac{\sigma_e}{\alpha}, \tag{24}$$

where α should be a number that is greater than 1.

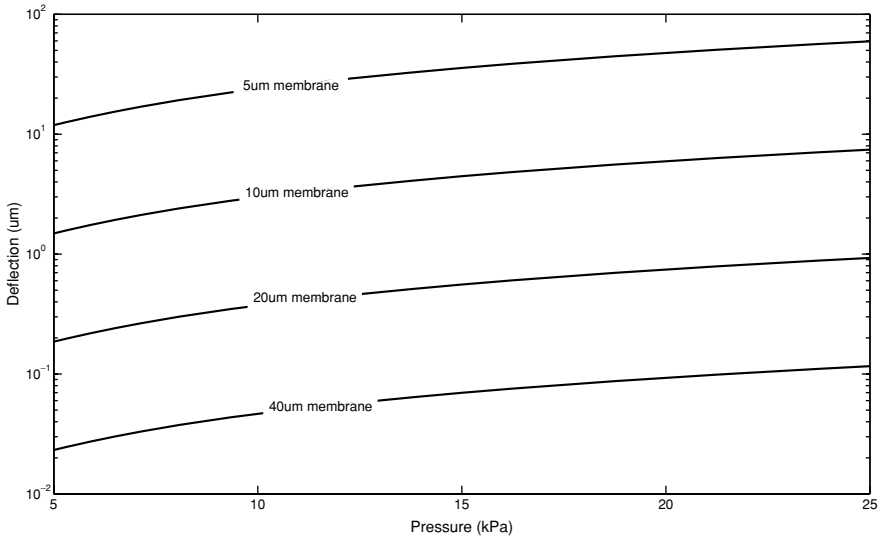

Fig. 13 Membrane deflection as a function of applied pressure for various thicknesses of membrane on a 1 mm diameter MEMS pressure sensor

It is interesting to note that the need for improved sensitivity suggests a thinner deflecting membrane, while the need for reliability suggests the need for a thicker substrate. Hence, the optimum design condition is the thickness that optimizes the deflection and the stresses in the membrane within the constraints implied by Eqs. (20) and (24).

Biocompatibility and adhesion/non-adhesion

One of the major obstacles to the use of long-term silicon in the body is the issue of biocompatibility and adhesion/non-adhesion [46, 53, 54]. The issue of biocompatibility has been studied by a number of investigators [46, 53, 54]. Some studies suggest adequate biocompatibility, while others suggest otherwise [54]. In any case, silicon is among the materials that can elicit cytotoxic response in the body. Hence, there is the need to consider the coating of silicon with biocompatible materials. Three approaches are considered in this paper.

Since titanium is one of the metals that have been shown to elicit no cytotoxic responses in the human body, the first approach involves the use of nano-scale titanium coatings in the improvement of the biocompatibility of silicon surfaces. This is considered in detail in a companion paper in this special issue [54]. This paper suggests that nano-scale Ti coatings with thicknesses of approximately 50 nm are sufficient to promote cell spreading and adhesion that is comparable to that observed on titanium surfaces [54]. However, the long term stability and corrosion behavior of these layers is yet to be studied in biological environments that simulate the behavior of body fluids. Nevertheless, the pasivating nature of surface oxide films on silicon and titanium surfaces suggests that the films should be durable in the chemically aggressive environment in the human body.

The second possible approach involves the use of polymeric layers, such as glycocalyx (see Fig. 14), as coatings on silicon. These have the advantages of being biocompatible. Glycocalyx is also known to reduce the adhesion of blood platelets to blood vessels. This is critical for the design of blood flow and platelet/surface interactions. However, the long term stability of glycocalyx and polymeric coatings is unclear. There may, therefore, be a need to engineer self healing polymeric layers that can replenish themselves over time. These are clearly challenges for future work.

The third approach is a combination of the first and the second approaches. The titanium coatings could then provide improved biocompatibility and corrosion resistance, while the upper polymeric or glycocalyx layers provide non-stick surfaces that do not adhere to blood platelets. These can be conjugated directly to amine groups that are attached to titanium surfaces using chemistry described in Milburn et al. [54].

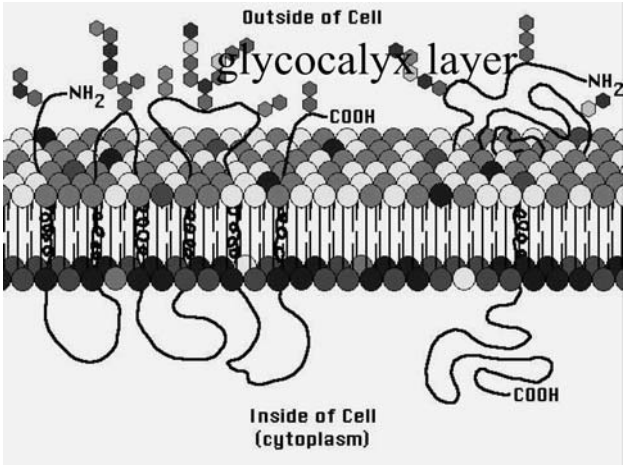

Fig. 14 Glycocalyx layer at cell surface

Implications/Conclusions

This paper presents analysis and ideas required for the design of implantable bio-MEMS pressure sensors. These include considerations of fluid flow, solid deformation and materials science associated with blood flow, deformation of fatty layers and blood vessels, biocompatibility, and the reliable sensing of blood pressure. A summary of the work is presented below along with salient conclusions arising from this study.

- The developed pressure equation provides a convenient method of estimating the degree of stenosis based on *in situ* pressure and flow measurements. However, two important effects are ignored in the current model: the dependence of the flow rate on the degree of stenosis and the fluid-structure interaction between the flow and elastic motion of the arteries. The change in flow rate through the graft due to the presence of the stenosis can be calculated either by modelling the system as a parallel circuit, or by assuming a constant energy loss through the graft branch of the circulatory system. The effect of fluid-structure interaction can be included by coupling the current CFD model with the axisymmetric material model.
- In the early stages of plaque formation, an *in vivo* blood pressure sensor will continue to measure blood pressure with some error in the reading due to the presence of the plaque. As the plaque thickens and stiffens over time, these measurements will become more unreliable. By coupling these measurements with additional data, such as from a flow sensor, diagnostic capabilities are significantly increased. The flow model discussed above can be used to determine the flow rates in the presence of various sizes of stenosis. These flow rates, coupled with the pressure data from the CFD model, can be used in conjunction with the pressure sensor and flow rate measurements to determine the actual degree of blockage in the stenosed graft.

- Diaphragm silicon pressure sensors with piezoelectric surface layers provide a robust platform for the design of implantable bio-MEMS sensors for the in-situ monitoring of blood flow. The sensors can be designed against fatigue by ensuring that their maximum stresses are below the fatigue endurance limits. The optimum structural thickness maximizes the pressure sensitivity without increasing the maximum the maximum membrane stresses above a fatigue design stress.
- The biocompatibility of silicon bio-MEMS structures can be improved by the use of nanoscale metallic titanium layers or polymeric layers such as glycocalyx. The nanoscale titanium layers promote improved biocompatibility and cell adhesion, while the glycocalyx layers can be used to tune the non-adhesion to blood platelets and the multiple constituents of blood. The combined use of nanoscale titanium coatings and glycocalyx layers is recommended for improved biocompatibility and non-adhesion of blood constituents.

While these models are simplifications of the actual complex behaviour of the blood flow, the visco-elastic behaviour of the stenosed artery, and the operation of the sensor, they demonstrate that bio-MEMS pressure sensors are legitimate candidates for use as *in vivo* blood pressure monitors. For a complete system to monitor the condition of a heart bypass graft, a magnetohydrodynamic (MHD) flow meter is also being developed. The MHD meter will consist of a pair of magnets and a set of electrodes oriented orthogonally around the exterior of the blood vessel. Voltage signals due to the MHD displacement current can be detected and interpreted to find flow rates in the graft. Coupled with a wireless transmitter, these sensors offer the possibility of long-term *in vivo* monitoring of bypass graft performance.

Acknowledgments The research is supported by the Division of Materials Research (Grant No. DMR 0231418) of the National Science Foundation. The authors are grateful to the Program Manager, Dr. Carmen Huber, for her encouragement and support.

References

1. T. MATSUDA, *Artif. Org.* **28**(1) (2004) 64.
2. Texas Heart Institute, Coronary bypass surgery (July 2004).
3. D. F. YOUNG, *J. Biomech. Eng.* **101** (1979) 157.
4. A. G. MAY, J. A. DEWEESE and C. G. ROB, *Surgery* **53** (1963) 513.
5. D. YOUNG, N. R CHOLVIN and A. C. ROTH, *Circ. Res.* **36** (1975) 735.
6. B. E. MORGAN, Flow through a model of an arterial stenosis, Master's thesis, (Iowa State University, 1971).
7. D. F. YOUNG and F. Y. TSAI, *J. Biomech.* **6** (1973) 395.
8. D. F. YOUNG and F. Y. TSAI, *J. Biomech.* **6** (1973) 547.
9. M. D. DESHPANDE, D. P. GIDDENS and R. F. MANBON, *J. Biomech.* **9** (1976) 165.
10. J. C. MISRA and S. CHAKRAVARTY, *J. Biomech.* **19** (1986) 907.
11. C. TU, M. DEVILLE and L. VANDERSCHUREN, *J. Biomech.* **25** (1992) 1141.
12. J. C. MISRA, M. K. PATRA and S. C. MISRA, *J. Biomech.* **26** (1993) 1129.
13. A.S. DVINSKY and M. OJHA, *Med. Biol. Eng. Comput.* **32** (1994) 138.
14. C. TU and M. DEVILLE, *J. Biomech.* **29** (1996) 899.
15. F. GHALICHI, X. DENG, A. DE CHAMPLAIN, Y. DOUVILLE, M. KING and R. GUIDOIN, *Biorheology* **35** (1998) 281.
16. D. BLUESTEIN, C. GUTIERREZ, M. LONDONO and R. T. SCHOEPHOERSTER, *Ann. Biomed. Eng.* **27** (1999) 763.
17. A. TURA and S. CAVALCANTI, *Comput. Biol. Med.* **31** (2001) 113.
18. F. MALLINGER and D. DRIKAKIS, *Biorheology* **39** (2002) 437.
19. S. S. VARGHESE and S. H. FRANKEL, *J. Biomech. Eng.* **125** (2003) 445.
20. L. GUOTAO, W. XIANJU, A. BAOQUAN and L. LIANGGANG, *Chinese J. Phys.* **42** (2004) 401.
21. D. TANG, J. YANG, C. YANG and D. N. KU, *J. Biomech. Eng.* **121** (1999) 494.
22. M. S. MOAYERI and G. R. ZENDEHBUDI, *J. Biomech.* **36** (2003) 525.
23. F. N. UNDERWOOD, A numerical study of the steady, axisymmetric flow through a disk-type prosthetic heart valve. Phd thesis, (University of Notre Dame, 1975).
24. F. N. UNDERWOOD and T. J. MUELLER, *J. Biomech. Eng.* (1977) 91.
25. F. N. UNDERWOOD and T. J. MUELLER, *J. Biomech. Eng.* **101** (1979) 198.
26. Y. C. FUNG, "Biomechanics: Mechanical Properties of Living Tissues" 2nd edn. (Springer-Verlag, New York, 1993).
27. C. S. ROY, *J. Physiol.* **3** (1880) 125.
28. D. H. BERGEL, *J. Physiol.* **156** (1961) 445.
29. D. J. PATEL, J. S. JANICKI and T. E. CAREW, *Circulation Research* **25** (1969) 765.
30. W. D. CASTLE and B. S. GOW, *Atherosclerosis* **47** (1983) 251.
31. B. S. GOW, W. D. CASTLE and M. J. LEGG, *J. Biomech.* **16**(6) (1983) 451.
32. T. MATSUMOTO, H. ABE, T. OHASHI, Y. KATO and M. SATO, *Physiol. Meas.* **23** (2002) 635.
33. H. M. LOREE, A. J. GRODZINSKY, S. Y. PARK, L. J. GIBSON and R. T. LEE, *J. Biomech.* **27**(2) (1993) 195.
34. K. HAYASHI and Y. IMAI, *J. Biomech.* **30**(6) (1997) 573.
35. N. V. SALUNKE and L. D. T. TOPOLESKI, *Crit. Rev. Biomech. Eng.* **25**(3) (1997) 243.
36. R. T. LEE, A. J. GRODZINSKY, E. H. FRANK, R. D. KAMM and F. J. SCHOEN, *Circulation* **83** (1991) 1764.
37. K. HAYASHI, *J. Biomech. Eng.* **115** (1993) 481.
38. R. T. LEE, S. G. RICHARDSON, H. M. LOREE, A. J. GRODZINSKY, S. A. GHARIB, F. J. SCHOEN and N. PANDIAN, *Arteriosclerosis Thromb.* **12** (1992) 1.
39. L. D. T. TOPOLESKI and N. V. SALUNKE, *Zeitschrift-furKardiologie* **89** (2000) (Suppl. 2):II/85–II/91.
40. Y. C. FUNG, "Biodynamics: Circulation," (Springer-Verlag, New York, 1984).
41. G. T. A. KOVACS, "Micromachined Transducers Handbook" (McGraw Hill, New York, 1998).
42. M. MADOU. "Fundamentals of Microfabrication" 2nd edn. (CRC Press, Boca Raton, FL, 2002).

43. K. BHALERAO, S. M. WENIFUMBO, A. B. O. SOBOYEJO and W. O. SOBOYEJO, *Nanotechnology* **6** (2004) 23.
44. S. TIMOSHENKO, "Theory of Plates and Shells" (McGraw Hill, New York, 1959).
45. W. N. SHARPE, S. BROWN, G. C. JOHNSON and W. KNAUSS, Round-robin tests of modulus and strength of polysilicon. In *Proc. Microelectromechanical Structures for Materials Research* (San Francisco, CA, 1998) p. 57.
46. B. D. RATNER, A. S. HOFFMAN, F. J. SCHOEN and J. E. LEMMONS, "Biomaterials Science: An Introduction to Materials Science in Medicine" 2nd edn. (Academic Press, San Diego, CA, 2004).
47. J. A. CONNALLY and S. B. BROWN, *Science* **256** (1992) 1537.
48. W. V. ARSDELL and S. BROWN, *J. Microelectromech. Syst.* **8** (1999) 319.
49. H. KAHN, R. BALLARINI, J. J. BELLANTE and A. H. HEUER, *Science* **298** (2002) 1215.
50. C. L. MUHLSTEIN, S. B. BROWN and R. O. RITCHIE, *J. Microelectromech. Syst.* **10** (2001) 593.
51. S. A. ALLAMEH, P. SHROTRIYA, A. BUTTERWICK, S. B. BROWN and W. O. SOBOYEJO, *J. Microelectromech. Syst.* **12** (2003) 313.
52. P. SHROTRIYA, S. ALLAMEH, S. B. BROWN, Z. SUO and W. O. SOBOYEJO, *Exper. Mech.* **43** (2003) 289.
53. D. M. BRUNETTE, P. TENGVALL, M. TEXTOR and P. THOMPSEN, "Titanium in Medicine: Materials Science, Surface Science, Engineering, Biological Responses and Medical Applications" (Springer, New York, 2001).
54. C. MILBURN, E. RUNG, G. M. OPARINDE, J. CHEN, A. C. BEYE, J. SCHWARTZ and W. O. SOBOYEJO, submitted to *J. Mater. Sci. Mater. Med.* (2004).